Non-Orthogonal Uplink Services Through Co-Transport of D-RoF/A-RoF in Mobile Fronthaul

Shuang Yao[®], You-Wei Chen[®], Shang-Jen Su[®], Yahya Alfadhli, Shuyi Shen[®], Rui Zhang[®], Qi Zhou[®], and Gee-Kung Chang, *Fellow*, *IEEE*, *Fellow*, *OSA*

Abstract—To efficiently support multiple services with diverse requirements in data capacity, latency, and connectivity in the fifth-generation (5G) communication system and beyond, various mobile fronthaul solutions, including digital and analog radioover-fiber (RoF), will be considered. We propose a non-orthogonal multiplexing scheme for multiservice uplink transmissions in mobile fronthaul, where in-band analog RoF (A-RoF) signals can be transmitted with digital RoF (D-RoF) signals simultaneously, resulting in high spectrum resource utilization. The demultiplexing is fulfilled by exploiting different characteristics of the D-RoF and A-RoF signals in the time-domain and it can be implemented with analog signal processing, providing low processing complexity and processing delay. The proposed scheme is experimentally demonstrated to achieve the joint transmission of the D-RoF and A-RoF signals over a shared mobile fronthaul through 20-km standard single mode fiber (SSMF). Experimental results show that in-band A-RoF signals from 2-10 GHz can be co-transmitted with D-RoF 10 GBaud NRZ-OOK signals, with the signal-to-interference-plusnoise ratio (SINR) enhanced by the demultiplexing module. Both received D-RoF and A-RoF signals can achieve bit error ratio (BER) lower than the 7% hard-decision forward-error correction (FEC) threshold.

Index Terms—Hybrid digital-analog transmission, mobile fronthaul, non-orthogonal division multiplexing.

I. INTRODUCTION

LONG with the development of the fifth-generation (5G) communication system, the centralized radio access network (C-RAN) has been investigated intensively over the past few years [1]–[3]. The baseband station (gNodeB) is split into three parts: central unit (CU), distributed unit (DU) and remote radio unit (RRU). This change in turn requires that the concepts of mobile fronthaul and midhaul to be re-defined as the network between DU and RRU, and that between CU and DU, respectively [4].

Manuscript received December 3, 2019; revised January 22, 2020 and March 8, 2020; accepted March 8, 2020. Date of publication March 12, 2020; date of current version July 20, 2020. This work was supported in part by a grant from Industry/University Cooperative Research program of National Science Foundation for Center of Fiber Wireless Integration and Networking (FiWIN) for Heterogeneous Mobile Communications under Contract 1539976. (Corresponding author: Shuang Yao.)

The authors are with the School of Electrical and Computer Engineering, Georgia Institute of Technology, Atlanta, GA 30308 USA (e-mail: syao65@gatech.edu; yu-wei.chen@ece.gatech.edu; taiwanjen@gatech.edu; yalfadhli@gatech.edu; ssyzoe@gatech.edu; ruizhangece@gatech.edu; qi.zhou@gatech.edu; geekung.chang@ece.gatech.edu).

Color versions of one or more of the figures in this article are available online at http://ieeexplore.ieee.org.

Digital Object Identifier 10.1109/JLT.2020.2980208

In the traditional 4G/LTE communication system, the mobile fronthaul utilizes CPRI [5] or OBSAI [6] protocol to transport digitized I/Q samples over the fiber. This solution requires high transmission capacity, especially when applied to massive multiple-input-multiple-output (M-MIMO) technology [1], [4]. In 5G, this issue is simplified by adding other functional split options, allowing a trade-off between fronthaul capacity and functional centralization to be optimized [7]. The ability to support different functional split options has been included as one important feature of eCPRI [8], an alternative solution to CPRI. However, eCPRI adopts the digital radio-over-fiber (D-RoF) technology, where the desired RF signals are transmitted as baseband signals with low spectral efficiency (SE). In addition, in order to comply with established frame format, (de)-packetization and (de)-compression have to be included. It will increase interface delay and thus is quite challenging to meet the latency requirements of mission-critical applications [9], [10]. On the other hand, analog radio-over-fiber (A-RoF), where the waveform of RF signals is preserved in the optical domain [11], does not require these operations. RF signals can be directly transmitted over fiber after electrical-to-optical conversion (E/O) [12], providing the desirable transparency of waveform and modulation format between optical fronthaul and free-space radio frequency (RF) transmission. Compared with D-RoF, A-RoF can achieve higher SE, simpler RRU design and higher flexibility in terms of dynamic capacity allocation [13].

As the next generation communication systems are evolving towards providing user-centric services, there will be no "one-size-fits-all" approach. Co-existence of various mobile fronthaul solutions are preferred, so that the merits of each solution can be fully exploited to meet the unique demands of user-centric services. To this end, both D-RoF and A-RoF techniques can be adopted to support system operations, as shown in Fig. 1. Therefore, a mobile fronthaul that supports co-delivery of the A-RoF and D-RoF signals over a shared fiber infrastructure is highly desirable.

Digital-analog signal hybrid transport in fiber-optic networks has been extensively studied in the cable television (CATV) system [14], [15]. With the emergence of 5G communication, it is commonly accepted as a promising solution to support wireless services overlay on the existing fixed networks [16]–[18]. In previously reported works, digital and analog signals were assigned with orthogonal resources, such as subcarrier multiplexing (SCM, Fig. 2(a)) [14], [16], or wavelength division multiplexing (WDM, Fig. 2(b)) [15]. A polarization division multiplexing (PDM) approach sketched in Fig. 2(c) [17] could be applied to improve the bandwidth utilization at the cost of an

0733-8724 © 2020 IEEE. Personal use is permitted, but republication/redistribution requires IEEE permission. See https://www.ieee.org/publications/rights/index.html for more information.

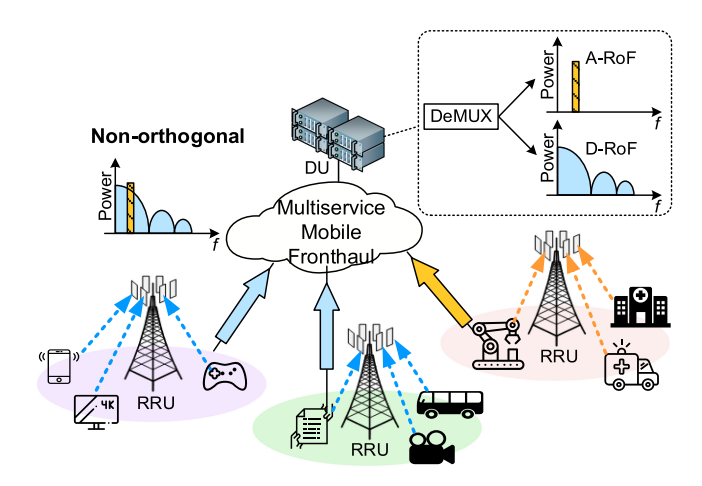


Fig. 1. Architecture of 5G mobile fronthaul.

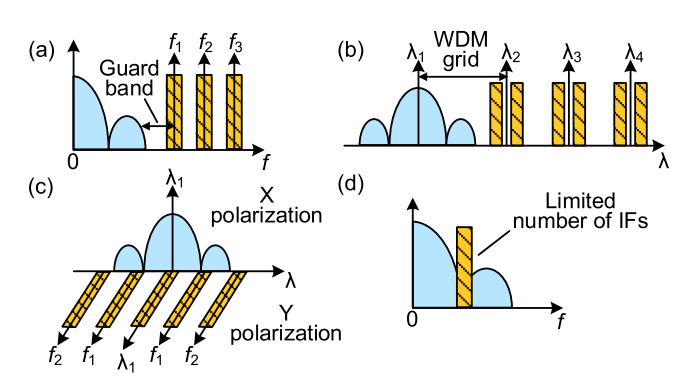


Fig. 2. Multiplexing in digital-analog hybrid transmission systems: (a) SCM; (b) WDM; (c) PDM; (d) A-RoF signals located at the null point of the D-RoF spectrum.

additional PDM demultiplexing scheme. In [18], by confining the A-RoF signals at the null point of the D-RoF spectrum, the guard band between the A-RoF signals and the D-RoF signals could be removed, as shown in Fig. 2(d). The interference is negligible under such frequency arrangement. However, the available intermediate frequencies (IFs) of A-RoF signals are limited, as is multiservice scalability. In this paper, the restrictions on the IFs are relaxed and the in-band A-RoF signals can co-exist with the D-RoF signals. To enable reliable co-delivery of the A-RoF and D-RoF signals in a shared mobile fronthaul, interference cancellation has to be included in the demultiplexing module. Rather than using successive interference cancellation (SIC) done by digital signal processing (DSP), interference cancellation in the analog domain is proposed, which takes advantages of the distinctive waveforms of the A-RoF and D-RoF signals. Moreover, the proposed method could be potentially DSP-free, economizing on processing delay and complexity. In such a scheme, the synchronization requirements between the D-RoF and A-RoF signals are relaxed, making it a promising solution for the uplink, meanwhile the digital-analog hybrid transmission method can be also adapted for the downlink.

In this paper, the principle of the proposed multiservice mobile fronthaul with A-RoF and D-RoF co-transmission is presented and verified through experiments. The bit-error ratio (BER) of the received D-RoF signals with and without the presence of the A-RoF signals is characterized in terms of the received optical

power (ROP) in both back-to-back (B2B) and 20-km standard single mode fiber (SSMF) transmission scenarios. For the A-RoF signals, the feasibility of the demultiplexing scheme is evaluated from the received spectra and the error vector magnitude (EVM). The optimal parameters of the system are also discussed, aiming at achieving a balance between the performances of those two kinds of signals. The scalability of the A-RoF signals is greatly extended and the available IFs can be between 2 and 10 GHz, when the D-RoF symbol rate is 10 GBaud, modulated with nonreturn-to-zero on-off-keying (NRZ-OOK). Therefore, it provides an 8-GHz workable region for IFs and is capable to support multiple 5G New Radio (5G-NR) bands, when each one is assigned with different IFs. Even though the received performance is degraded due to the residual interference among them, with -7.5 dBm maximum received power, the achievable power margin in the most critical scenario can still be 12.5 dB and 11.8 dB for the D-RoF and A-RoF signals, respectively. Therefore, the proposed non-orthogonal multiservice uplink is a promising solution for mobile fronthaul with high reliability and flexibility.

II. OPERATING PRINCIPLES

The operating principles are illustrated in Fig. 3. For the RRU adopting D-RoF techniques, received wireless signals are down-converted to baseband and digitized in the RF layer. Digitized bits are then mapped to NRZ-OOK symbols. For the RRUs deploying A-RoF techniques, received 5G-NR signals are directly up-converted or down-converted to the IFs. The D-RoF and A-RoF signals are multiplexed and then passed through the shared mobile fronthaul for upstream transmission.

At the DU, the received signals are sent into the demultiplexing module, where they are split into a D-RoF branch and an A-RoF branch. The first stages in both branches are optical-to-electrical conversion (O/E). The analog electrical signals after these two O/E devices are denoted as $y_{PD,1}(t)$ and $y_{PD,2}(t)$, respectively. They are directly used for interference cancellation without digital-to-analog conversion (DAC). In the D-RoF branch, a limiting amplifier (LA) comes after the O/E device, which is commonly used in the OOK receiver to shape pulse [19], [20]. It has a high small-signal gain that can assist in decision when the received signals are small. When the input signals have detected voltages higher than the threshold voltage $V_{\rm th}$, the output of LA will saturate and thus "limiting" the output voltage [20]. If the combined waveform of the D-RoF and A-RoF signals are dominated by OOK signals, whether the detected voltage is larger than $V_{
m th}$ mainly depends on the D-RoF signals. Therefore, the A-RoF signals can be suppressed by the LA and the LA output signals $y_{LA}(t)$ can be directly used for D-RoF decoding, the same way as the commonly used D-RoF receivers. In the A-RoF branch, we make use of $y_{LA}(t)$ to extract the A-RoF signals. $y_{LA}(t)$ can be viewed as a reconstruction of the original D-RoF signals. Thus, we can recover the A-RoF signals by subtracting $y_{LA}(t)$ from $y_{PD,2}(t)$. It is similar to SIC, as the interference cancellation is performed by reconstruction and subtraction. However, the proposed scheme is implemented in the analog domain with negligible processing delay. The attenuator in the lower branch is used to adjust the gain differences of two branches, i.e., the

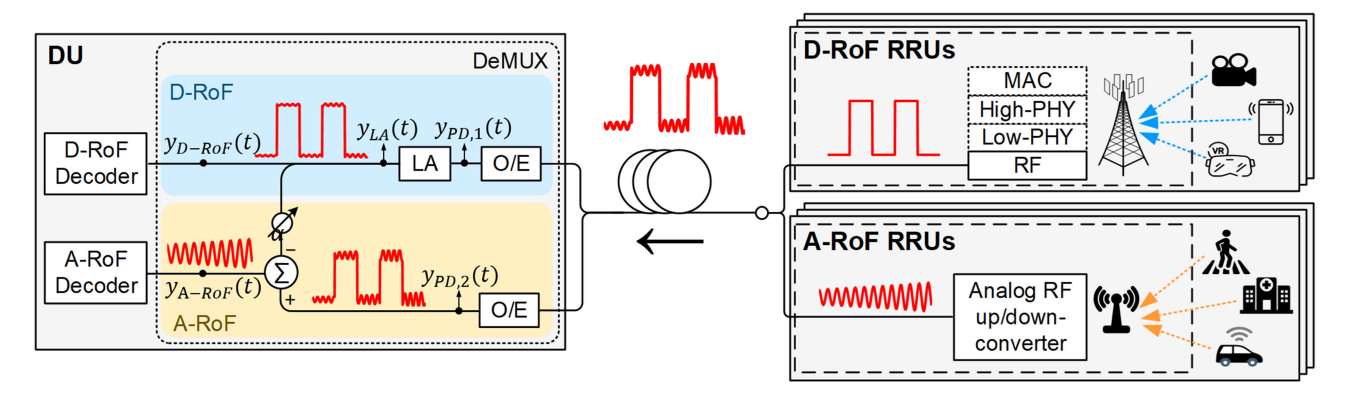


Fig. 3. Operating principles of co-delivery of D-RoF and A-RoF.

signals used for D-RoF and A-RoF decoding are:

$$y_{D-RoF}(t) = y_{LA}(t) \tag{1}$$

$$y_{A-RoF}(t) = y_{PD,2}(t) - \alpha y_{LA}(t)$$
 (2)

where α is the attenuation factor of the attenuator.

It is clear from Eq. (1) and (2) that $y_{LA}(t)$ plays a crucial role in the demultiplexing. To ensure that the LA can extract a "clean" version of D-RoF signals, Eq. (3) must be satisfied:

$$|a_{D-RoF}| - |a_{A-RoF}| > V_{th} \tag{3}$$

where $a_{\mathrm{D-RoF}}$ is the amplitude of the D-RoF signals and $a_{\mathrm{A-RoF}}$ is the maximum amplitude of the A-RoF signals. Therefore, one safe option is to make $a_{\mathrm{D-RoF}}$ large while keeping $a_{\mathrm{A-RoF}}$ small. On the other hand, to conquer the intensity noise, such as thermal noise and shot noise, the amplitude of the A-RoF signals cannot be too small to maintain the signal-to-noise ratio (SNR), which serves as the lower bound of $a_{\mathrm{A-RoF}}$.

Orthogonal frequency-division multiplexing (OFDM) has been formalized by the 3rd Generation Partnership Project (3GPP) as the modulation format for 5G. OFDM signals have a high peak-to-average power ratio (PAPR) and symbols with large amplitude only compromise a small portion of the transmitted symbols. Under most circumstances, it might be too conservative to use maximum amplitude of the A-RoF signals in Eq. (3). One alternative is to use the standard deviation of the A-RoF signals $\sigma_{\text{A-RoF}}$. Since the OFDM symbols are a sum of modulated subcarriers, the probability density function (PDF) of the amplitudes approximate a Gaussian distribution when the number of carriers is larger than 64, according to the central limit theorem [21]. Therefore, the maximum amplitude of the A-RoF signals in Eq. (3) can be replaced with $k \cdot \sigma_{\text{A-RoF}}$, where the value of k depends on the specific requirements of the system.

III. EXPERIMENTAL SETUP

The experimental setup is shown in Fig. 4. D-RoF and A-RoF data are generated offline and sent to an arbitrary waveform generator (AWG, Keysight, M8195A) running at 30 GSa/s. Generated D-RoF and A-RoF signals are amplified by two driver amplifiers respectively. The D-RoF and A-RoF signals can be combined in the electrical or optical domain. Here the signals are combined in the electrical domain using a power combiner. The multiplexed signals are modulated onto a 1550 nm optical carrier through a Mach-Zehnder modulator (MZM) biased at quadrature

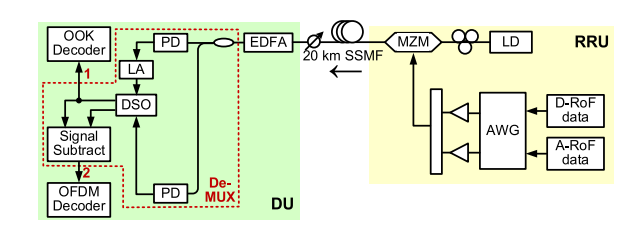


Fig. 4. Experimental setup (LD: laser diode, PD: photodiode).

point for intensity modulation. The polarization controller (PC) is used to adjust the polarization of continuous lightwave before entering the MZM. The modulated optical signal is transmitted over 20-km SSMF, resulting in -7.5 dBm maximum received power. At the DU, the combined received signals are first pre-amplified by an erbium-doped fiber amplifier (EDFA) to compensate for the transmission loss and then enter the demultiplexing module (DeMUX). In the DeMUX, the received signals are split into two branches by a 3-dB coupler. The upper branch corresponds to the D-RoF branch mentioned in Section II, while the bottom branch is the A-RoF branch. Signal subtraction in Eq. (2) could be implemented in the analog domain by a differential amplifier. However, due to device limitation, we subtract $y_{LA}(t)$ from $y_{PD,2}(t)$ in the Matlab after the received signals get digitized. Hence, a digital sampling oscilloscope (DSO) is also included in the DeMUX in the experimental demonstration. The DSO (Keysight, DSOZ254A) captures the signals from both branches simultaneously at 40 GSa/s. The output ports 1 and 2 of the DeMUX correspond to Eq. (1) and (2), respectively. Synchronization, down-sampling and decision are implemented in the D-RoF decoder module. While for A-RoF decoding, down-conversion, down-sampling, synchronization, Fast Fourier Transform (FFT), frequency domain equalization and QAM demodulation are performed sequentially.

The baud rate of NRZ-OOK signals is 10 GBaud, giving a raw data rate of 10 Gbps. For the OFDM signals, the subcarrier spacing is 240 KHz and the FFT size is 2048 with a CP length of 144. 1200 subcarriers are loaded with data and occupy 288 MHz bandwidth. The modulation format for each subcarrier is quadrature phase shift keying (QPSK).

IV. RESULTS AND DISCUSSION

When the IF of the A-RoF signals is 10 GHz, the power spectrum density (PSD) of $y_{PD,2}(t)$ and $y_{LA}(t)$ are depicted in

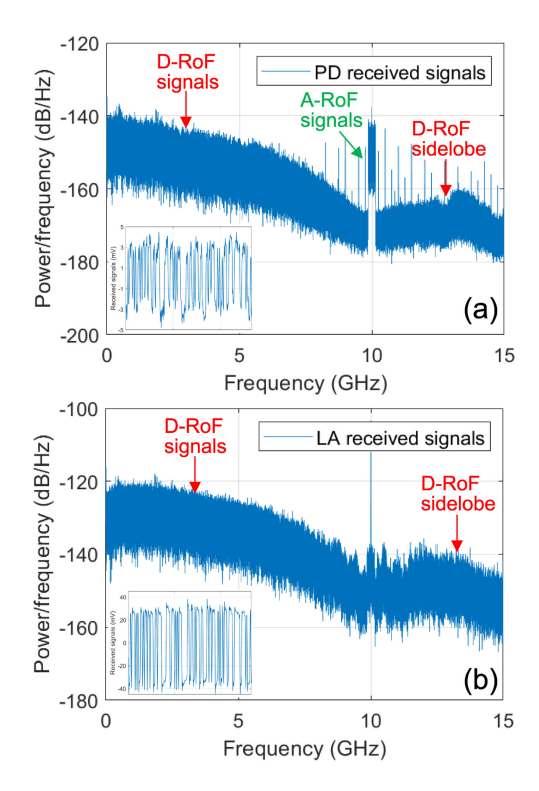


Fig. 5. The signal spectra when ${\rm IF}=10~{\rm GHz}$: (a) after the PD, (b) after the LA.

Fig. 5(a) and (b), respectively, with insets showing the snapshots of the signals in the time domain. It can be seen from the inset of Fig. 5(a) that the amplitudes of the A-RoF signals are relatively small compared to those of the D-RoF signals, so the major part of the D-RoF signals' waveform is preserved and the spectrum still follows a *sinc* function, with a null point at 10 GHz. Although the A-RoF signals can be hardly seen in the time domain, it is more visible in the frequency-domain, due to the frequency arrangement. After the LA, amplitude variations are reduced and the waveform becomes more "square-like", as the inset of Fig. 5(b) illustrates. Waveform overshoot is mainly attributed to the limited bandwidth of the employed devices. It is clear from Fig. 5(b) that the shaping of LA greatly suppresses the A-RoF signals and regenerates the D-RoF signals with a tone at 10 GHz. Therefore, it is promising to extract the A-RoF signals by the following signal subtraction.

Fig. 6 depicts the BER versus the ROP for the D-RoF and A-RoF signals. The constellation diagrams for the A-RoF signals at ROP of -21.5 dBm are shown in the insets. Measured results for both B2B and after 20-km SSMF transmission are shown, and the cases where there are only D-RoF or A-RoF signals are also shown as benchmarks. In the case of the D-RoF signals, as the A-RoF signals can almost be suppressed to the noise floor by the LA, the power penalty of introducing the A-RoF signals is less than 0.5 dB. There is no power penalty introduced by a 20-km SSMF transmission and the sensitivity at 7% hard-decision forward-error correction (HD-FEC) BER threshold $(3.8 \times 10^{-3}, [22])$ is -25.5 dBm. In the case of the A-RoF signals, due to the minimal power of the D-RoF signals at 10 GHz, the signal-to-interference-plus-noise ratio (SINR) can still be kept high even if the D-RoF signals are transmitted at the

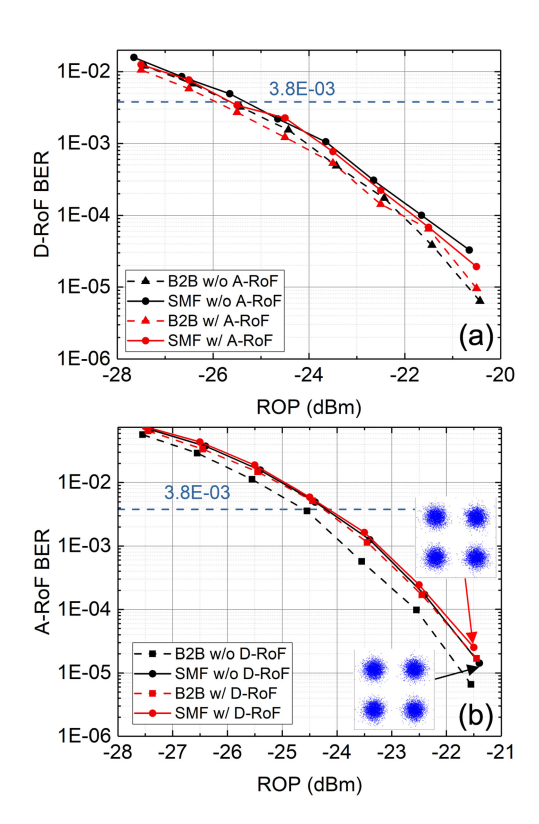


Fig. 6. BER versus ROP in B2B and after 20-km SSMF transmission when IF =10 GHz: (a) D-RoF signals; (b) A-RoF signals with insets showing constellation diagrams when ROP =-21.5 dBm.

same time. Therefore, only $y_{PD,2}(t)$ is employed for OFDM demodulation, i.e., the α in Eq. (2) is set to 0. The lowest BER is achieved when only A-RoF signals are transmitted in the B2B scenario, exhibiting about 0.5 dB ROP improvement compared with the other three cases. The penalties of fiber transmission are negligible and the sensitivity at 7% HD-FEC BER threshold is -24.5 dBm.

As mentioned before, by applying the proposed signal demultiplexing method, the in-band A-RoF signals can co-exist with the D-RoF signals. Therefore, we experiment with IFs being 20%, 40%, 60% and 80% of the baud rate, i.e., 2 GHz, 4 GHz, 6 GHz and 8 GHz. Fig. 7 shows the PSD of the received signals when IF is 2 GHz or 8 GHz, where the system is expected to experience the worst or the least interference, respectively. In both trials with IF of 2 or 8 GHz, the ROP is fixed at -11.5 dBm after 20-SSMF transmission. The first row of Fig. 7 (Fig. 7(a), (b)) depicts the spectrum of $y_{PD,2}(t)$, the second row (Fig. 7(c)–(d)) being $y_{LA}(t)$ and the third row (Fig. 7(e)–(f)) being $y_{A-RoF}(t)$ acquired by applying Eq. (2). It is worth mentioning that the performances of the proposed signal demultiplexing method largely depend on the amplitudes of the D-RoF and A-RoF signals and the α in Eq. (2). For now, the amplitudes are kept unchanged and the α is optimized as we change IFs and their impact will be discussed later. In comparing Fig. 7(a)–(b) with the Fig. 7(c)–(d), it is clear that the LA can suppress the A-RoF signals by a large amount and enhance the tone at 10 GHz, which will facilitate the clock recovery and demodulation of the D-RoF signals. This kind of suppression can occur in both cases, since the voltages of the received signals are kept larger than the $V_{\rm th}$ of the LA, no matter which IF

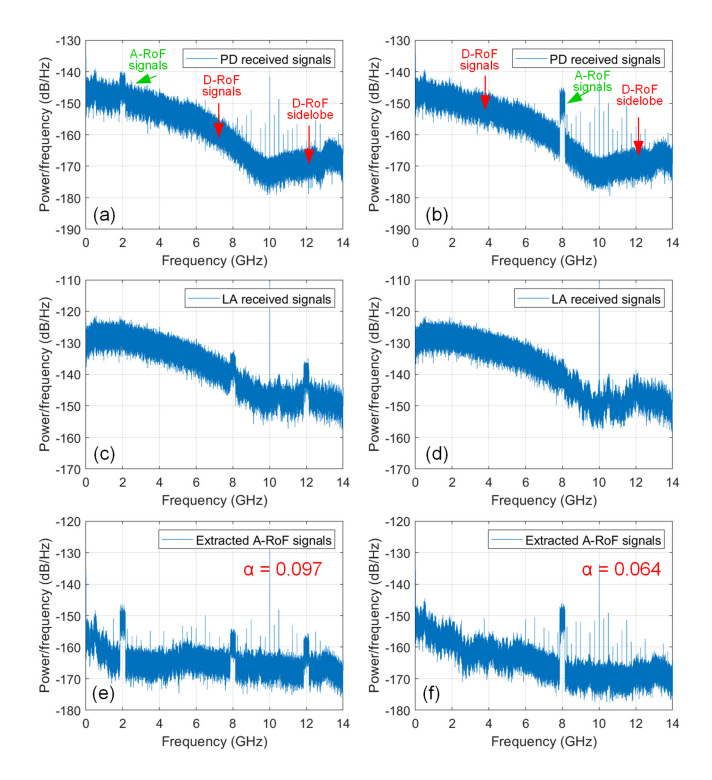


Fig. 7. The signal spectra when ROP is -11.5 dBm: (a)–(b): after the PD, (c)–(d) after the LA; (e)–(f) extracted A-RoF signals; for figures (a), (c), (e) IF = 2 GHz; for figures (b), (d), (f) IF = 8 GHz.

is being used. Therefore, Fig. 7(c)–(d) exhibit similar spectra, yet they actually correspond to the cases with different IFs. Furthermore, as the A-RoF components in $y_{LA}(t)$ are reduced, subtracting $y_{LA}(t)$ from $y_{PD,2}(t)$ can greatly improve the SINR of the A-RoF signals, as illustrated in Fig. 7(e)–(f). And the SINR improvements take place in all the tested cases, too. Along with the enhancement of the A-RoF signals, a large portion of the D-RoF components in the $y_{PD,2}(t)$ are also removed, which can be seen by comparing Fig. 7(e)–(f) with Fig. 7(a)–(b).

The artifacts near 8 GHz and 12 GHz in Fig. 7(e) are due to the beating between the tone at 10 GHz and the A-RoF signals. They also carry the A-RoF data yet have worse EVM as the result of lower SINR. These artifacts also exist for other IFs, say at 2 GHz and 18 GHz when the IF is 8 GHz, but is insignificant in the spectra due to the higher power of the D-RoF signals and the limited bandwidth of the receiver.

To further investigate the performances of the demultiplexing method, we compare the EVM of the A-RoF signals when $y_{PD,2}(t)$ and $y_{A-RoF}(t)$ are used for decoding, respectively. The results are shown in Fig. 8. The cases where the A-RoF signals are transmitted alone are also shown for references. Again, the demultiplexing method is capable of mitigating interference when IFs take on values of 2, 4, 6, 8 GHz and the EVM of the A-RoF signals gets improved accordingly. The improvement is more notable with lower IFs. At lower IFs, the A-RoF signals suffer from serious interference and exhibits low SINR, because there is more power distributed at the lower frequencies of the D-RoF spectrum. When only $y_{PD,2}(t)$ is used, the A-RoF signals can be barely demodulated. The EVM at ROP being -11.5 dBm and IF being 2 GHz is 104.5%, while it can be

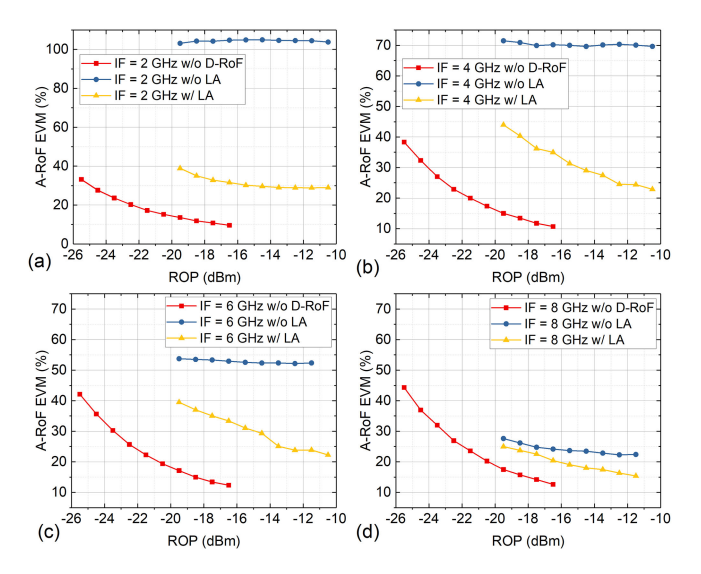


Fig. 8. EVM of the A-RoF signals with and without the presence of the D-RoF signals, with and without LA. (a) IF = 2 GHz; (b) IF = 4 GHz; (c) IF = 6 GHz; (d) IF = 8 GHz.

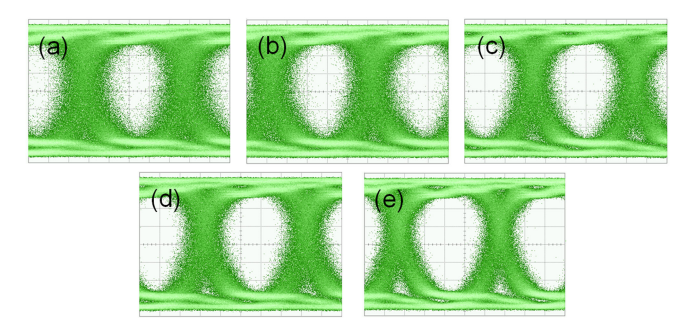


Fig. 9. Eye diagrams of $y_{LA}(t)$ when ROP = -21.5 dBm: (a) IF = 2 GHz; (b) IF = 4 GHz; (c) IF = 6 GHz; (d) IF = 8 GHz; (e) IF = 10 GHz.

significantly reduced to 28.8% under the same circumstance if $y_{A-RoF}(t)$ is demodulated.

Another observation from Fig. 8 is that the EVM remains almost the same as ROP increase, when only $y_{PD,2}(t)$ is used for demodulation. This indicates that the system is mainly limited by interference from the D-RoF signals and thus launching more power cannot bring about better performances. On the other hand, for $y_{A-RoF}(t)$, the degradation from interference is lessened and the resulting SINR arises from the combined effect of residual interference and intensity noise inherent to the system. Therefore, performances can be partly compensated by increasing ROP. Taking this into consideration, we can allocate IFs to RRUs accordingly. The RRUs with shorter distances to DUs or better channel conditions can be assigned with lower IFs. while those with longer distances or worse channel conditions will be assigned with higher IFs. Fig. 9 shows the eye diagrams of $y_{LA}(t)$ when IF is 2, 4, 6, 8,10 GHz. As IF decreases, the D-RoF signals become more jittery, because the D-RoF spectrum increasingly overlaps with the in-band A-RoF signals. This accounts for the degradation of both D-RoF and A-RoF signals. As Eq. (2) suggests, if the D-RoF signals cannot be reconstructed with high accuracy, the A-RoF signals will also be negatively affected.

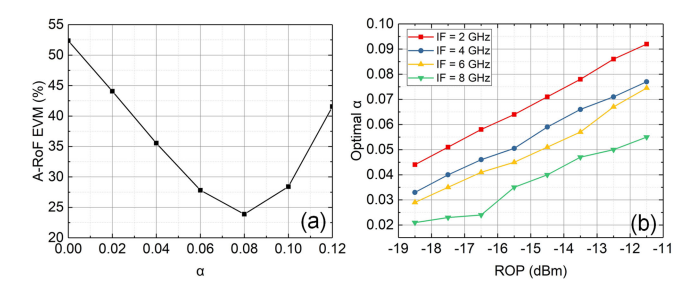


Fig. 10. (a) EVM of the A-RoF signals versus α when IF = 8 GHz, ROP = -11.5 dBm; (b) optimal α versus ROP under different IFs.

As mentioned previously, the attenuation factor α plays an essential role in the demodulation of A-RoF signals. Under fixed ROP, varying α exerts the similar effect on all IFs. Here we only show the case where IF is 8 GHz and ROP is -11.5 dBm, and the EVM versus α is illustrated in Fig. 10(a). In our experiment, α is much less than 1 because the LA amplifies D-RoF signals while suppressing the A-RoF signals at the same time. According to Eq. (2), values of α have to be chosen properly to make sure that the D-RoF components can be removed correctly. Therefore, as Fig. 10(a) shows, the EVM will decrease as α increases when it is between 0 and 0.08. Once α is greater than 0.08, the EVM will be degraded with larger α , as the D-RoF signals are now added back.

Fig. 10(b) depicts the optimal α versus ROP under different IFs. Due to the nonlinear behavior of LA, the output voltage is fixed at the highest output level once the input voltage is higher than the $V_{\rm th}$. On the other hand, the PD has a linear response. As ROP decreases, the output voltage of PD decreases linearly, while the output voltage of LA remains almost the same, thus smaller α should be used to correct for the gain differences in these two branches. It can also be seen from Fig. 10(b) that higher IFs require smaller α . This is mainly because the two branches have different frequency response. When we use Eq. (2) to extract A-RoF signals, α is optimized to minimize the in-band interference. Thus, as shown in Fig. 7(f), there is still residual interference in the low frequency part when α is optimized to get the lowest EVM.

The relative amplitude of the D-RoF and A-RoF signals is another important parameter determining the performance of the system Fig. 11 illustrates the BER of the D-RoF signals and the EVM of the A-RoF signals as a function of the peak-topeak voltage (V_{DD}) of the input to the D-RoF signals' driver amplifiers. As discussed in Section II, the amplitude of the D-RoF signals has to be large enough to make sure that the voltage of the received signals is higher than the $V_{\rm th}$ of the LA. Fig. 11(a) shows that the BER of D-RoF signals decrease with higher $V_{\rm pp}$, as the D-RoF components make up an increasing proportion of the received signals and the difference between $|a_{D-RoF}| - |a_{A-RoF}|$ and $V_{\rm th}$ increases. Consequently, the LA does a better job in reconstructing the D-RoF signals. However, the A-RoF signals present different performances. Although an improvement in D-RoF reconstruction can lead to a lower EVM, higher V_{DD} also means that there are less power occupied by the A-RoF signals, keeping ROP unchanged. In other words, the SINR of the A-RoF signals will be smaller. Under these two opposing effects, the EVM of the A-RoF signals slightly increases as $V_{\rm pp}$ becomes larger, as shown in Fig. 11(b). In

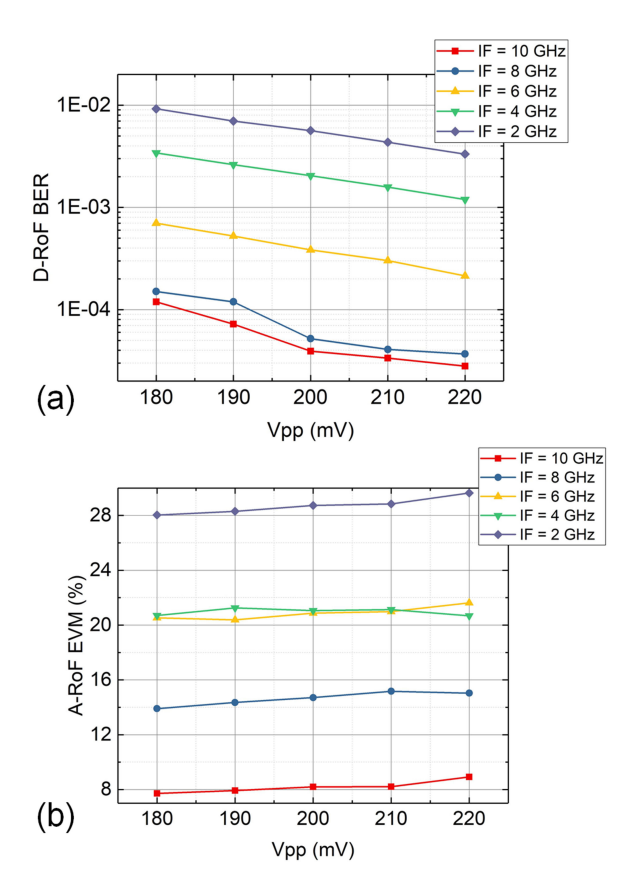


Fig. 11. (a) BER of the D-RoF signals versus $V_{\rm pp}$ under different IFs (ROP = -21.5 dBm); (b) EVM of the A-RoF signals versus $V_{\rm pp}$ under different IFs (ROP = -13.5 dBm).

reality, the power allocation between the D-RoF and A-RoF signals should be optimized to guarantee that both can achieve adequate SINR for following up processing.

Fig. 12 shows the BER versus ROP for the D-RoF and A-RoF signals as IFs take on values of 2, 4, 6, 8 GHz, with $V_{\rm DD}$ of 200 mV and optimal α . There is no power penalty induced by 20-km SSMF transmission for both D-RoF and A-RoF signals under all four cases. The BER curves cross the 7% HD-FEC BER threshold in all the tested scenarios, demonstrating feasibility of the proposed scheme. For the D-RoF signals, the BER increases when IF gets lower, which agrees with the results presented previously. And the BER can also be improved by using higher ROP. This is because there are two kinds of impairments in the system: residual interference and intensity noise, and they impact the system differently under different conditions. With lower IFs, the slope of BER-ROP curve is smaller since the D-RoF signals suffer from more interference. However, as ROP decreases, the intensity noise gradually dominates the impairments and the gaps between different BER curves shrinks. When ROP is smaller than -25.5 dBm, the cases with IF of 6 GHz and 8 GHz achieve similar performances. The sensitivities at 7% HD-FEC BER threshold for IF being 2, 4, 6, 8 GHz are -20.0 dBm, -23.5 dBm, -25.5 dBm and -25.5 dBm, respectively. In the case with the most serious interference, the power margin, which is defined as the power difference between fiber output and the received sensitivity, is 12.5 dB with the SSMF output power being -7.5 dBm.

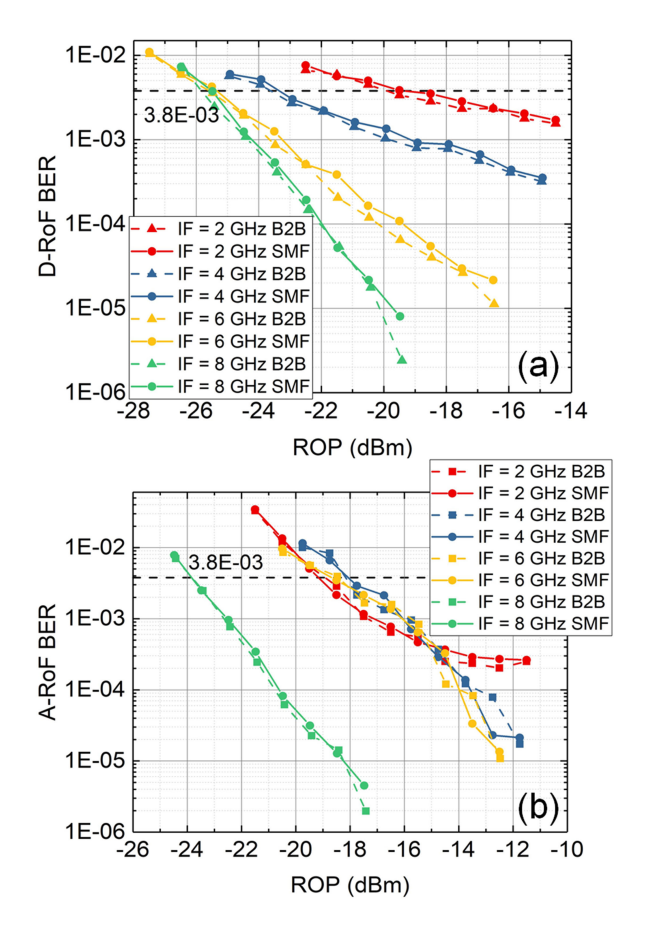


Fig. 12. BER versus ROP under different IFs. (a) D-RoF signals; (b) A-RoF signals.

In the case of the A-RoF signals, as explained previously, the dominating interference are reduced to the similar level of intensity noise after the demultiplexing module. Therefore, the BER decreases with ROP increases. The case with IF being 8 GHz presents lower BER than the other cases, because it is able to achieve higher SINR, as can be seen from Fig. 7(e)–(f). Similar to the D-RoF signals, when ROP is lower than -14.5 dBm, the intensity noise becomes the major limiting factor and the BER for the cases with IFs being 2, 4, 6 GHz are almost the same. On the other hand, there exists an error floor when ROP is larger than -12.5 dBm with IF of 2 GHz, which implies that the residual interference becomes the bottleneck of the system under this condition. The sensitivities at 7% HD-FEC BER threshold for IF being 2, 4, 6, 8 GHz are $-19.3 \, dBm$, $-18.5 \, dBm$, $-18.2 \, dBm$ and -23.8 dBm, respectively. Therefore, the worst-case power margin for the A-RoF signals is 11.8 dB, as the SSMF output power is -7.5 dBm.

V. CONCLUSION

In this paper, we have proposed a non-orthogonal multiservice uplink system for 5G mobile fronthaul based on co-transport of D-RoF/A-RoF, where the D-RoF and A-RoF signals can be used to fulfill the diverse demands of different services. The proposed demultiplexing method decomposes the received signals into the D-RoF and A-RoF components, while mitigating the interference from non-orthogonal multiplexing at the same time. It ex-

tends the usable range of IFs for the A-RoF signals, adding more scalability to the proposed scheme. The feasibility is verified via experiments by transmitting both D-RoF and A-RoF signals through the shared 20-km SSMF. When the D-RoF signals is 10 GBaud NRZ-OOK symbols, the IFs for the A-RoF signals can be allocated at 2–10 GHz, and they can be agilely assigned to RRUs based on the differences in received SINR. In conclusion, the proposed multiservice uplink system is a promising candidate to realize co-delivery of the D-RoF and A-RoF signals, with low complexity and high resource utilization.

REFERENCES

- X. Liu, H. Zeng, N. Chand, and F. Effenberger, "Efficient mobile fronthaul via DSP-based channel aggregation," *J. Lightw. Technol.*, vol. 34, no. 6, pp. 1556–1564, Mar. 2016.
- [2] T. Pfeiffer, "Next generation mobile fronthaul and midhaul architectures," J. Opt. Commun. Netw., vol. 7, no. 11, pp. B38–B45, Nov. 2015.
- [3] J. S. Wey and J. Zhang, "Passive optical networks for 5G transport: Technology and standards," *J. Lightw. Technol.*, vol. 37, no. 12, pp. 2830–2837, Jun. 2019.
- [4] "Transport network Support of IMT-2020/5G," ITU Telecommun., Geneva, Switzerland, Tech. Rep. GSTR-TN5G, Feb. 2018.
- [5] Common Public Radio Interface, Interface specification, V7.0, Oct. 2015.
- [6] Open Base Station Architecture Initiative, BTS system reference document, V2.0, 2016.
- [7] "Radio access architecture and interfaces," 3GPP, Sophia Antipolis Cedex, France, TR38.801, V2.0.0, R14, Mar. 2017.
- [8] eCPRI, "Common public radio interface: ECPRI interface specification," V1.2, Jun. 2018.
- [9] C.-Y. Chang, R. Schiavi, N. Nikaein, T. Spyropoulos, and C. Bonnet, "Impact of packetization and functional split on C-RAN fronthaul performance," in *Proc. IEEE Int. Conf. Commun.*, May 2016.
- [10] Y. Alfadhli et al., "Latency performance analysis of low layers function split for URLLC applications in 5G networks," Comput. Netw., vol. 162, Oct. 2019, Art. no. 106865.
- [11] "Radio-over-fibre (RoF) technologies and their applications," ITU Telecommun., Geneva, Switzerland, Tech. Rep. ITU-T G Suppl. 15, Jul 2015
- [12] C. Liu, L. Zhang, M. Zhu, J. Wang, L. Cheng, and G. Chang, "A novel multi-service small-cell cloud radio access network for mobile backhaul and computing based on radio-over-fiber technologies," *J. Lightw. Tech*nol., vol. 31, no. 17, pp. 2869–2875, Sep. 2013.
- [13] J. E. Mitchell, "Integrated wireless backhaul over optical access networks," J. Lightw. Technol., vol. 32, no. 20, pp. 3373–3382, Oct. 2014.
- [14] W. I. Way, "Subcarrier multiplexed lightwave system design considerations for subscriber loop applications," *J. Lightw. Technol.*, vol. 7, no. 11, pp. 1806–1818, Nov. 1989.
- [15] W. I. Way et al., "Simultaneous distribution of multichannel analog and digital video channels to multiple terminals using high-density WDM and a broad-band in-line erbium-doped fiber amplifier," *IEEE Photon. Technol. Lett.*, vol. 2, no. 9, pp. 665–668, Sep. 1990.
- [16] X. Hu et al., "Converged mobile fronthaul and passive optical network based on hybrid analog-digital transmission scheme," in Proc. Opt. Fiber Commun. Conf., Mar. 2016, Paper W3C.5.
- [17] S. Shen et al., "Polarization-tracking-free PDM supporting hybrid digitalanalog transport for fixed-mobile system," *IEEE Photon. Technol. Lett.*, vol. 31, no. 1, pp. 54–57, Jan. 2019.
- [18] C. Browning *et al.*, "5G wireless and wired convergence in a passive optical network using UF-OFDM and GFDM," in *Proc. IEEE Int. Conf. Commun. Workshops*, May 2017, pp. 386–392.
- [19] P. H. Binh, V. D. Trong, P. Renucci and X. Marie, "Improving OOK modulation rate of visible led by peaking and carrier sweep-out effects using n-schottky diodes-capacitance circuit," *J. Lightw. Technol.*, vol. 31, no. 15, pp. 2578–2583, Aug. 2013.
- [20] E. Sackinger and W. C. Fischer, "A 3-GHz 32-dB CMOS limiting amplifier for SONET OC-48 receivers," *IEEE J. Solid-State Circuits.*, vol. 35, no. 12, pp. 1884–1888, Dec. 2000.
- [21] J. Armstrong and A. J. Lowery, "Power efficient optical OFDM," *Electron. Lett.*, vol. 42, no. 6, pp. 370–372, Mar. 2016.
- [22] "Forward error correction for high bit-rate DWDM submarine systems," ITU Telecommun., Geneva, Switzerland, ITU-T G.975.1, Feb. 2004.